Coupled heat and mass transfer in biosourced porous media without local equilibrium: A macroscopic formulation tailored to computational simulation

Patrick Perre

Version of Record: https://www.sciencedirect.com/science/article/pii/S0017931018363658
Manuscript_9729e9f83cda5208bf13ff97850816e5

Coupled heat and mass transfer in biosourced porous media without local equilibrium : a macroscopic formulation tailored to computational simulation.

Patrick Perré [a,b,*]

[a] *LGPM, CentraleSupélec, Université Paris-Saclay, 8-10 rue Joliot-Curie, 91 190 Gif-sur-Yvette, France*

[b] *LGPM, CentraleSupélec, Centre Européen de Biotechnologie et de Bioéconomie (CEBB), 3 rue des Rouges Terres, 51 110 Pomacle, France*

Abstract

This paper proposes a macroscopic formulation of coupled heat and mass transfer that can consider non-local equilibrium often encountered in biosourced building materials (wood- and plant-fiber based materials). Transferring dual-scale effects and molecular relaxation at the macroscopic level involves a kernel function acting in a convolution product. To ease the computational solution of the set of equations, the memory function is decomposed as a series of exponential functions. Each function yields an internal variable that obeys a simple ordinary differential equation (ODE). This paper first describes the macroscopic and dual-scale formulations used as reference solutions. Subsequently, the modified macroscopic formulation of coupled transfer and its computational solution are presented in detail. The major outcomes of the present study, validated against reference solutions obtained with a comprehensive dual-scale model, are as follows:

- Dual-scale diffusion can be approached accurately by two exponential functions,
- Even though the dual-scale phenomenon and molecular relaxation do not occur at the same scale, both can be considered in the modified macroscopic formulation of coupled transfer additively,
- The new macroscopic formulation, together with the computational procedure proposed in this study, can be applied to various configurations, namely coupled heat and mass transfer in packed beds.

Keywords:
abnormal diffusion, building energy simulation, dual-scale modeling, molecular relaxation, multiscale modeling, non-Fickian, packed bed, transient state, wood

1. Introduction

The thermal performance standards of buildings are becoming increasingly demanding that designers and architects require simulation tools to achieve remarkable accuracy [11, 49, 12]. In the meantime, as they offer good performances with a reduced ecological

*Corresponding author
Email address: patrick.perre@centralesupelec.fr (Patrick Perré)

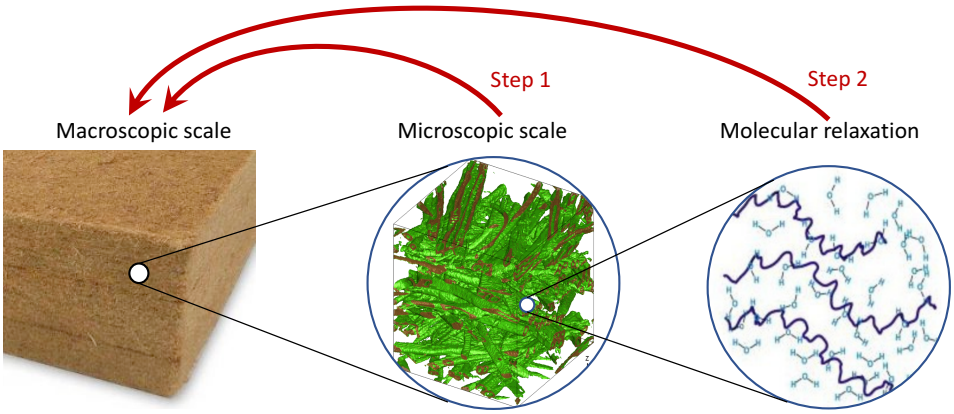

Figure 1: In lignocellulosic materials, memory effects during transient hydric changes arise owing to dual-scale mechanisms and molecular relaxation. This study proposes a macroscopic formulation able to account for both phenomena.

footprint, biosourced materials are used increasingly in construction. As these materials exhibit an important moisture buffering effect, building energy simulation (BES) models must account for coupled heat and mass transfer, thus resulting in a strong demand for mass transfer characterization. This includes mass diffusivity and sorption isotherms [20, 18], but should also include more subtle effects that affect the moisture buffering capacity. For example, it is well known that the sorption behavior depends on the hydric history of the materials [13, 7]. This sorption hysteresis affects the energy demand of a building [21] and must be considered in BES models [14, 38]. Similarly, non-Fickian behaviors of bound water diffusion in fibrous materials such as fiberboards have been reported. This is revealed, for example, by a slow shift in moisture content during the relative humidity (RH) plateau after a sudden change [22] or a dependence of the mass diffusion coefficient with the sample thickness [37].

These abnormal behaviors are attributed to two phenomena arising at different spatial scales (Fig. 1): dual-scale MC fields at the fiber scale and relaxation at the macromolecular scale:

- **Dual-scale effects** are likely to occur in heterogeneous materials structured as a connected conductive phase and a storage phase. Depending on the sample size and imposed conditions, this microstructure may produce local equilibrium failures [19, 24, 27, 28].
- **Molecular relaxation** in polymers has been reported more than six decades ago [9]. Re-arrangement at the macromolecular state when a penetrant diffuses into a polymer substance requires some time, depending on the macromolecular mobility. Such effects exist in biomacromolecules [7, 46].

These problems of fading memory were indicated when simulating transfer in insulation materials: the identified transfer parameters depend on the experimental information used (local RH or moisture content) [4]. Similarly, the dimensionless diffusivity identified for LDF using the RH value at the back face of the sample was greater than that of the unit, which is non-physical [34, 29]. The classical formulation of coupled heat and mass transfer therefore cannot represent the experimental facts. Recently, a simple approach

was proposed to address this question partially. The long delay required to reach the equilibrium asymptotically has been represented well by modifying the boundary conditions. A delayed relation between the external relative humidity and the surface moisture content was introduced. The formulation involves an exponential function defined by a time constant and a non-Fickian proportion [25, 26]. By modifying the formulation at the boundary, one assumes implicitly that all points of the materials have the same history, which is a strong assumption. Consequently, this representation is valid only if the time constant for diffusion in the material thickness remains much smaller than the related relaxation time constant.

The crucial need for a general and rigorous framework able to include non-local equilibrium in the macroscopic formulation of coupled heat and mass transfer is the primary motivation of the present study. This paper is organized as follows. The comprehensive macroscopic formulation of coupled heat and mass is presented first. The complete dual-scale formulation, based on distributed micro-models, is summarized as well. This model will be used later for validation purposes. Subsequently, the central section of the paper describes the development of the rigorous framework: a new formulation able to account for non-Fickian effects in the set of coupled macroscopic equations. The related computational strategy is also presented in detail as this is mandatory for the formulation to be used in computational codes, namely in BES models. This strategy includes a simple, yet accurate, method to account for bound water diffusion inside the microscopic inclusions.

This framework is subsequently validated using the comprehensive dual-scale model. Using full dual-scale simulations as reference tools allowed for two important points to be verified: the ability of the reduced model to account for diffusion in the inclusions and the possibility to couple two mechanisms arising at different spatial scales. This last section proves that both effects (dual-scale fields and molecular relaxation) can be transferred successfully and simultaneously at the macroscopic scale (the two arrows in Fig. 1).

2. Theoretical models

2.1. Macroscopic formulation

The comprehensive set of macroscopic equations was derived using the volume averaging procedure [42, 15, 47, 48]. The development of the volume-averaged transport equations requires the existence of a representative elementary volume (REV) V that is sufficiently large to smooth the microscopic fluctuations and sufficiently small to avoid macroscopic variations. Two average operators are defined on this REV, namely, the superficial average and the intrinsic average. For example, the superficial average of the density of the liquid phase is given by

$$\overline{\rho}_w = \frac{1}{V} \int_{V_w} \rho_w \, dV \tag{1}$$

and the intrinsic average is expressed as

$$\overline{\rho}_w^w = \frac{1}{V_w} \int_{V_w} \rho_w \, dV \tag{2}$$

where V_w is the volume of the liquid phase contained in V. Further, the relationship $\overline{\rho}_w = \varepsilon_w \overline{\rho}_w^w$ in which $\varepsilon_w = V_w/V$ is the volume fraction of the liquid phase.

The full set of equation, as proposed by [47, 48] and adapted to the case of hygroscopic products [31, 32] reads as follows:

Moisture conservation

$$\frac{\partial\left(\varepsilon_w\rho_w+\varepsilon_g\overline{\rho}_v^g+\overline{\rho}_b\right)}{\partial t}+\nabla\cdot\left(\rho_w\overline{\boldsymbol{v}}_w+\overline{\rho}_v^g\overline{\boldsymbol{v}}_g+\overline{\rho_b\boldsymbol{v}}_b\right)=\nabla\cdot\left(\rho_g\boldsymbol{D}_{eff}\cdot\nabla\omega_v\right) \tag{3}$$

Energy conservation

$$\begin{aligned}\frac{\partial}{\partial t}&\left(\varepsilon_w\rho_w h_w+\varepsilon_g(\overline{\rho}_v^g h_v+\overline{\rho}_a^g h_a)+\overline{\rho_b h_b}+\varepsilon_s\rho_s h_s-\varepsilon_g p_g\right)\\&+\nabla\cdot\left(\rho_w h_w\overline{\boldsymbol{v}}_w+(\overline{\rho}_v^g h_v+\overline{\rho}_a^g h_a)\overline{\boldsymbol{v}}_g+h_b\overline{\rho_b\boldsymbol{v}}_b\right)+\overline{\boldsymbol{v}}_w\cdot\nabla p_w+\overline{\boldsymbol{v}}_g\cdot\nabla p_g\\&=\nabla\cdot\left(\rho_g\boldsymbol{D}_{eff}(h_v\nabla\omega_v+h_a\nabla\omega_a)+\boldsymbol{\lambda}_{eff}\nabla T\right)\end{aligned} \tag{4}$$

The transport of enthalpy due to bound water migration must be treated with care. As the differential heat of sorption depends on the bound water content, the averaged value $\overline{h}_b$ should be used in the time evolution (accumulation term), whereas the value at ρ_b (h_b) should be used in the migration term, as it is assumed that the less bound water molecules are those likely to migrate.

Air conservation

$$\frac{\partial\left(\varepsilon_g\overline{\rho}_a^g\right)}{\partial t}+\nabla\cdot\left(\overline{\rho}_a^g\overline{\boldsymbol{v}}_g\right)=\nabla\cdot\left(\rho_g\boldsymbol{D}_{eff}\nabla\omega_a\right) \tag{5}$$

In these equations, the barycentric mass velocities are from the generalized Darcy's law:

$$\begin{aligned}\overline{\boldsymbol{v}}_g&=-\frac{\boldsymbol{K}\boldsymbol{k}_g}{\mu_g}(\nabla p_g-\rho_g\nabla\psi_{\boldsymbol{g}})\\\overline{\boldsymbol{v}}_w&=-\frac{\boldsymbol{K}\boldsymbol{k}_w}{\mu_w}(\nabla p_w-\rho_w\nabla\psi_{\boldsymbol{g}})\quad with\quad P_w=P_g-P_c(X,T)\end{aligned} \tag{6}$$

The bound water flux is expressed using the bound water density as the driving force:

$$\begin{aligned}\overline{\rho_b\boldsymbol{v}}_b&=-\boldsymbol{D}_b\nabla\overline{\rho}_b=-\rho_0\boldsymbol{D}_b\nabla X_b\\\text{where}\quad X_b&=min(X,X_{fsp})\end{aligned} \tag{7}$$

Boundary conditions

$$\begin{aligned}\boldsymbol{J}_v|_{x=0^+}\cdot\boldsymbol{n}&=h_m\,c\,M_v\,\ln\left(\frac{1-x_\infty}{1-x_v|_{x=0}}\right)\\\boldsymbol{J}_h|_{x=0^+}\cdot\boldsymbol{n}&=h_h\left(T|_{x=0}-T_\infty\right)\\P_g|_{x=0^+}&=P_{atm}\end{aligned} \tag{8}$$

The first boundary equation assumes that only water vapor is exchanged between the product and the surrounding air. The two first boundary equations are involved in the enthalpy balance at the boundary.

This macroscopic formulation assumes that the porous medium is locally at equilibrium:

A1 the temperature is the same for all phases $T_s = T_w = T_g$

A2 the partial pressure of water vapor inside the gaseous phase is related to the moisture content X *via*, and the sorption isotherm $p_v = p_{vs}(T) \times a_w(T, X)$, where function a_w is the sorption isotherm of the product, also called water activity, namely in food science.

Further assumptions allow this set of equations to have a more convenient form:

A3 the variation in partial densities inside the REV are negligible; therefore, the intrinsic average is equal to the local value $\overline{\rho}_v^g = \rho_v$ and $\overline{\rho}_a^g = \rho_a$,

A4 the solid density is assumed to be constant $\rho_s = constant$,

A5 the moisture content X is used to consider the total amount of water present in the porous medium $\rho_0 X = \varepsilon_w \rho_w + \varepsilon_g \overline{\rho}_v^g + \overline{\rho}_b$ where $\rho_0 = \epsilon_s \rho_s$,

A6 the effective diffusivity is expressed as a function of the binary diffusivity of vapor in air: $\boldsymbol{D}_{eff} = \boldsymbol{f}\boldsymbol{D}_v$, where $\boldsymbol{f}$ is a dimensionless diffusivity tensor (indeed, along one given direction, $f = 1/\mu$ where μ is the vapor resistance ratio used for building materials),

A7 the study related to pressure variations can be omitted in the enthalpy balance.

With these additional assumptions, the set of equations becomes:

Moisture conservation

$$\rho_0 \frac{\partial X}{\partial t} + \nabla \cdot (\rho_w \overline{\boldsymbol{v}}_w + \rho_v \overline{\boldsymbol{v}}_g) = \nabla \cdot (\rho_g \boldsymbol{f}\boldsymbol{D}_v \nabla \omega_v + \rho_0 \boldsymbol{D}_b \nabla X_b) \tag{9}$$

Energy conservation

$$\begin{aligned} \frac{\partial}{\partial t} \left(\varepsilon_w \rho_w h_w + \varepsilon_g (\rho_v h_v + \rho_a h_a) + \overline{\rho_b h_b} + \varepsilon_s \rho_s h_s \right) & \\ + \nabla \cdot (\rho_w h_w \overline{\boldsymbol{v}}_w + (\rho_v h_v + \rho_a h_a) \overline{\boldsymbol{v}}_g) & \\ = \nabla \cdot (\boldsymbol{\lambda}_{eff} \nabla T + (h_v - h_a) \rho_g \boldsymbol{f}\boldsymbol{D}_v \nabla \omega_v + h_b \rho_0 \boldsymbol{D}_b \nabla X_b) & \end{aligned} \tag{10}$$

Air conservation

$$\frac{\partial (\varepsilon_g \rho_a)}{\partial t} + \nabla \cdot (\rho_a \overline{\boldsymbol{v}}_g) = \nabla \cdot (\rho_g \boldsymbol{f}\boldsymbol{D}_v \nabla \omega_a) \tag{11}$$

2.2. Dual-scale formulation

As already stated in the introduction, coupled transfer in heterogeneous media could lead the failure of local equilibrium (assumptions **A1** and **A2** of the previous section). This is particularly true when the medium consists of a connected conductive phase and a slow storage phase. In the case of building materials, a low-density fiberboard (LDF) is a typical example of such morphology regarding mass transfer. This is also required when a thick bed of particles is involved [33]. In such cases, a dual-scale approach is mandatory: the

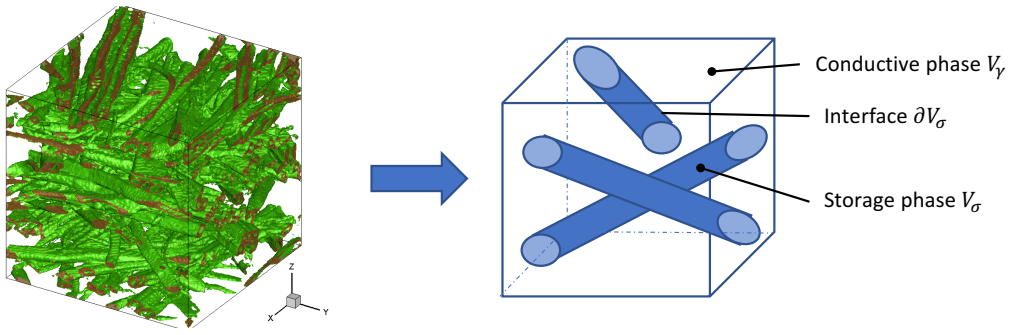

Figure 2: Low-density fiber boards (LDFs) consist of a highly connected gaseous phase, a conductive phase, and a highly hygroscopic solid phase that acts as the storage phase. In the dual-scale approach, the real morphology of the LDF as observed by microtomography (left), is approached by a representative elementary volume (REV) consisting of a set of long cylinders of the same radius r.

two spatial scales must be computed simultaneously, for example, using the concept of distributed microstructure models [40].

Classical two-scale approaches for flow in porous media assume that at each point in the macroscopic domain, a unit cell exists that is representative of the underlying pore geometry at that point. A set of transport equations is proposed to describe the global (macroscopic) flow, and a separate set of equations is used to describe the local (microscopic) flow. The typical two-scale coupling strategy [17, Ch. 9 by R. E. Showalter] and [3, 8, 43] is to impose the macroscopic values on the microscopic field via Dirichlet boundary conditions, and to include a source term at the macroscopic level that represents the exchange of fluid (from the microscale to the macroscale) across the unit cell boundary. This so-called distributed micro-model approach is well adapted provided that the storage phase does not contribute to the macroscopic fluxes. Although more sophisticated approaches have been proposed to account for the contribution of the storage phase to the macroscopic fluxes [5], the classical formulation is used in this study, as it is well adapted to the LDF. However, the formulations proposed in the literature cannot accommodate the coupling between heat and mass transfers that is important when evaporation or condensation occurs. To overcome this problem, we used a comprehensive formulation proposed by the author [27, 28]. This formulation is suitable for distributed microstructure models in the case of coupled heat and mass transfer, considering the total gaseous pressure through the balance equation of dry air. Therefore, the proposed set of equations involves three independent state variables, at both the macroscopic and microscopic scales. In the following equations, superscript γ denotes the macroscopic scale, and superscript σ denotes the microscopic scale. In order to avoid the confusion with the intrinsic phase of the considered scale, the scale superscript is shifted to the right when a superficial average is involved (for example, $\overline{v}_g{}^{\sigma}$ instead of $\overline{v}_g^{\sigma}$). Ω designs the macroscopic domain, V_σ is the part of the REV V occupied by the storage phase, and ∂V_σ is the interface between the conductive and storage phase inside V. Two space coordinates systems are involved: $\mathbf{x}$ denotes the macroscopic position in Ω, and $\mathbf{y}$ is the position inside the REV V at point $\mathbf{x}$.

Microscopic scale

Moisture conservation

$$\rho_0 \frac{\partial X^\sigma}{\partial t} + \nabla_y \cdot (\rho_w^\sigma \overline{\boldsymbol{v}}_w{}^\sigma + \rho_v^\sigma \overline{\boldsymbol{v}}_g{}^\sigma)$$
$$= \nabla_y \cdot \left(\rho_g^\sigma \boldsymbol{D}_{eff}^\sigma \nabla_y \omega_v^\sigma + \rho_0^\sigma \boldsymbol{D}_b^\sigma \nabla X_b^\sigma\right) \quad y \in V_\sigma(x),\ x \in \Omega \tag{12}$$

Energy conservation

$$\frac{\partial}{\partial t}\left(\varepsilon_w^\sigma \rho_w^\sigma h_w^\sigma + \varepsilon_g^\sigma(\rho_v^\sigma h_v^\sigma + \rho_a^\sigma h_a^\sigma) + \overline{\rho_b h_b}^{\,\sigma} + \varepsilon_s^\sigma \rho_s^\sigma h_s^\sigma - \varepsilon_g^\sigma P_g^\sigma\right)$$
$$+ \nabla_y \cdot (\rho_w^\sigma h_w^\sigma \overline{\boldsymbol{v}}_w{}^\sigma + (\rho_v^\sigma h_v^\sigma + \rho_a^\sigma h_a^\sigma)\overline{\boldsymbol{v}}_g{}^\sigma)$$
$$= \nabla_y \cdot \left(\boldsymbol{\lambda}_{eff}^\sigma \nabla_y T^\sigma + (h_v^\sigma - h_a^\sigma)\rho_g^\sigma \boldsymbol{D}_{eff}^\sigma \nabla_y \omega_v^\sigma + h_b^\sigma \rho_0^\sigma \boldsymbol{D}_b^\sigma \nabla X_b^\sigma\right) \quad y \in V_\sigma(x),\ x \in \Omega \tag{13}$$

Air conservation

$$\frac{\partial}{\partial t}\left(\varepsilon_g^\sigma \rho_a^\sigma\right) + \nabla_y \cdot (\rho_a^\sigma \overline{\boldsymbol{v}}_g{}^\sigma) = \nabla_y \cdot \left(\rho_g^\sigma \boldsymbol{D}_{eff}^\sigma \nabla_y \omega_a^\sigma\right) \quad y \in V_\sigma(x),\ x \in \Omega \tag{14}$$

Macroscopic scale

In the following equations, moisture is assumed to be present only as water vapor in the conductive phase.

Moisture conservation

$$\frac{\partial}{\partial t}\left(\varepsilon_g^\gamma \rho_v^\gamma\right) + \nabla_x \cdot (\rho_v^\gamma \overline{\boldsymbol{v}}_g{}^\gamma) = \nabla_x \cdot \left(\rho_g^\gamma \boldsymbol{D}_{eff}^\gamma \nabla_x \omega_v^\gamma\right) + Q_v(t,x) \quad x \in \Omega \tag{15}$$

Energy conservation

$$\frac{\partial}{\partial t}\left(\varepsilon_g^\gamma(\rho_v^\gamma h_v^\gamma + \rho_a^\gamma h_a^\gamma)\right) + \nabla_x \cdot ((\rho_v^\gamma h_v^\gamma + \rho_a^\gamma h_a^\gamma)\overline{\boldsymbol{v}}_g{}^\gamma)$$
$$= \nabla_x \cdot \left(\rho_g^\gamma \boldsymbol{D}_{eff}^\gamma (h_v^\gamma \nabla_x \omega_v^\gamma + h_a^\gamma \nabla_x \omega_a^\gamma) + \lambda_{eff}^\gamma \nabla_x T^\gamma\right)$$
$$+ Q_h(t,x) + h_v^\gamma Q_v(t,x) + h_a^\gamma Q_a(t,x) \quad x \in \Omega \tag{16}$$

Air conservation

$$\frac{\partial}{\partial t}\left(\varepsilon_g^\gamma \rho_a^\gamma\right) + \nabla_x \cdot (\rho_a^\gamma \overline{\boldsymbol{v}}_g{}^\gamma) = \nabla_x \cdot \left(\rho_g^\gamma \boldsymbol{D}_{eff}^\gamma \nabla_x \omega_a^\gamma\right) + Q_a(t,x) \quad x \in \Omega \tag{17}$$

Coupling between scales

A two-way coupling holds between the microscopic and macroscopic scales: the boundary conditions applied at the local scale involve the macroscopic variables, and the integration of the fluxes on the contour of the micro-model builds up the source terms to be supplied at the macroscopic level. These couplings are summarized hereinafter:

Moisture exchange

$$\begin{aligned}
&\rho_g^\sigma \boldsymbol{D}_{eff}^\sigma \nabla_y \omega_v^\sigma \cdot \boldsymbol{n} = h_m^\sigma \rho_g^\sigma \ (\omega_v^\sigma(t,x,y) - \omega_v^\gamma(t,x)) \quad y \in \partial V_\sigma(x), \quad x \in \Omega \\
&Q_v(t,x) = \frac{1}{|V|} \int_{\partial V_\sigma(x)} \rho_g^\sigma \boldsymbol{D}_{eff}^\sigma \nabla_y \omega_v^\sigma \cdot \boldsymbol{n} \, dS \quad x \in \Omega
\end{aligned} \tag{18}$$

Heat exchange

$$\begin{aligned}
&\lambda_{eff}^\sigma \nabla_y T^\sigma \cdot \boldsymbol{n} = h_h^\sigma \left[T^\sigma(t,x,y) - T^\gamma(t,x)\right] \quad y \in \partial V_\sigma(x), \ x \in \Omega \\
&Q_h(t,x) = \frac{1}{|V|} \int_{\partial V_\sigma(x)} \lambda_{eff}^\sigma \nabla_y T^\sigma \cdot \boldsymbol{n} \, dS \quad x \in \Omega
\end{aligned} \tag{19}$$

Air exchange

$$\begin{aligned}
&P^\gamma(t,x) = P^\sigma(t,x,y) \quad y \in \partial V \sigma(x), \ x \in \Omega \\
&Q_a(t,x) = \frac{1}{|V|} \int_{V_\sigma} \frac{\partial \rho_a^\sigma}{\partial t} dV \quad x \in \Omega
\end{aligned} \tag{20}$$

3. Macroscopic formulation of memory effects

Memory effects occurring at microscopic scales have important effects at the macroscopic scale, and are typically revealed by a non-Fickian behavior: the macroscopic field does not obey the Fickian law for moisture transport. The aim of this study is to propose, test, and validate a macroscopic formulation able to consider these memory effects. Two major effects encountered in bio-based building materials are considered:

- Molecular relaxation: owing to the mobility of macromolecules, new sorption sites appear with the reorganization of molecules after a change in bound water content [9]. For lignocellulosic materials, this is particularly observable at high levels of relative humidity or for thermally modified products [46, 26],
- Dual-scale effects: owing to the long characteristic time of diffusion in the secondary cell wall, the local equilibrium sometimes fails. At the macroscopic level, this induces a delay between the change in air characteristics and the moisture content of the product, even at the extremely fine microscopic scale.

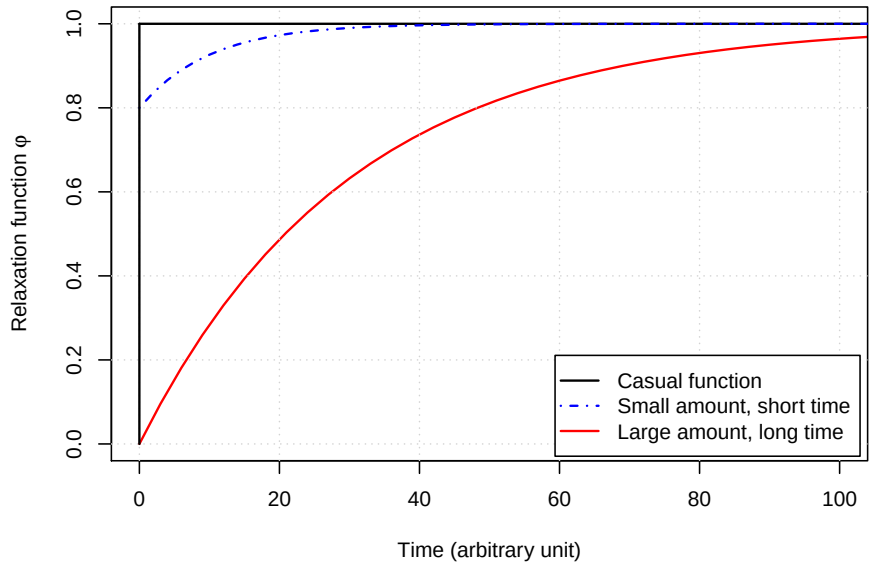

Figure 3: Some possible shapes of the relaxation function.

3.1. Molecular relaxation

This phenomenon can be approached using a relaxation function, defined by applying a sudden change in RH surrounding the product at the microscopic scale, from RH_{ini} to RH_{fin}, assuming the product to be at equilibrium at $t = 0$ ($X_{ini} = X_{eq}(RH_{ini})$). In this case, the evolution of the local moisture content is simply the signature of molecular relaxation:

$$X(t) - X_{ini} = \Delta X_{eq} \times \varphi(t) \tag{21}$$

where ΔX_{eq} is defined by the sorption isotherm values: $\Delta X_{eq} = X_{eq}(RH_{fin}) - X_{eq}(RH_{ini})$ and φ a monotonic function such that $\lim \varphi(t)_{t\to\infty} = 1$.

It is obvious from equation (21) that if φ is the casual function (the Heaviside function, see figure 3), any memory effect vanishes.

In a more general case, the value of RH surrounding the product varies over time; therefore, a convolution product is required:

$$X(t) - X_{ini} = \int_0^t \varphi(t-\tau)\frac{\partial X_{eq}}{\partial \tau} d\tau \tag{22}$$

where

$$\frac{\partial X_{eq}}{\partial \tau} d\tau = dX_{eq} \tag{23}$$

represents the variation in equilibrium moisture content during the infinitesimal time interval $d\tau$.

In practice, the function φ can be determined experimentally by submitting a minute sample to a sudden change in the external relative humidity. For computational purposes, it is convenient to approach the experimental function as a sum of exponential functions:

$$\varphi(t) = 1 - \sum_{i=1}^{N} \alpha_i exp(-t/\tau_i) \tag{24}$$

In practice, one single exponential function is sufficient to capture the trend determined using relevant experiments [6].

3.2. *Dual-scale effects*

Similar macroscopic effects can arise from dual-scale phenomena: depending on the characteristic time for the moisture field to equilibrate at the microscopic scale, a delay might exist between the equilibrium moisture content and the actual moisture content. This is known as the failure of the local thermodynamic equilibrium. For example, we can refer to the mass diffusion in a cylindrical fiber of radius R. By neglecting the resistance to mass transfer in the gaseous phase of the porous medium, the equilibrium moisture content X_{eq} can be used as the Dirichlet boundary conditions at the solid phase surface. In the case of a perfectly cylindrical shape, for example, the corresponding analytical solution can be used: [10]

$$X(r,t) - X_{ini} = \Delta X_{eq} \times \left(1 - \frac{2}{R} \sum_{i=1}^{\infty} \frac{exp(-D\alpha_i^2 t) J_0(r\alpha_i)}{\alpha_i J_1(R\alpha_i)}\right) \tag{25}$$

where the values of α_n are the positive roots of

$$J_0(R\,\alpha_n) = 0 \tag{26}$$

where $J_0(x)$ and J_1 are the Bessel functions of the first kind of orders zero and one, respectively.

The integration of equation (25) over the cylinder volume allows for the average moisture content $\bar{X}$ to be obtained:

$$\bar{X}(t) - X_{ini} = \Delta X_{eq} \times \left(1 - \sum_{i=1}^{\infty} \frac{4}{R^2\alpha_i^2} exp(-D\alpha_i^2 t)\right) \tag{27}$$

A function φ, similar to that proposed for molecular relaxation (21), can be deduced from equation (27):

$$\varphi(t) = 1 - \sum_{i=1}^{\infty} \frac{4}{R^2\alpha_i^2} exp(-D\alpha_i^2 t) \tag{28}$$

To compute sufficient terms in equation (28), an algorithm based on the Newton method was written in R to obtain the roots of J_0 with an accuracy of 1.10^{-10}. Using 500 terms, the error at origin, i.e., the worst case, is already good ($\varphi(0) < 10^{-3}$). Similar expressions are available for plates or spheres [10]. Figure 4 compares the solutions obtained for three simple inclusion shapes (plate, cylinder, and sphere). As will be shown in the next section, the form of the analytical solutions (infinite sum of exponential functions) is not suitable

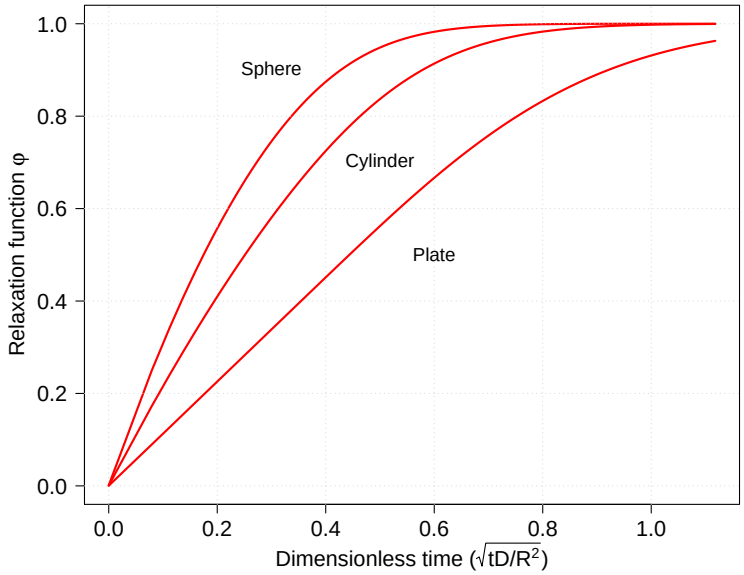

Figure 4: Dimensionless change in moisture content. Result obtained for different shapes using the first 500 terms of the respective analytical solutions [10].

Table 1: Parameter values to approach diffusion in a simple-shape inclusion with one exponential function (the identification was performed over the dimensionless time interval $[0, 1.2]$ and with 500 terms of the analytical solutions).

Parameters	**Plate**	**Cylinder**	**Sphere**
α_1	0.85818	0.81243	0.80684
$\tau_1/(a^2/D)$	0.38373	0.14990	0.07921
Norm of residues	39.10^{-3}	58.10^{-3}	62.10^{-3}

for computational algorithms. These solutions were therefore approached by one or two exponential functions:

$$\varphi(t) = 1 - \sum_{i=1}^{N} \alpha_i exp(-t/\tau_i), \quad \text{with } N = 1 \text{ or } 2 \tag{29}$$

A simple truncation of the infinite sum of the analytical solution (28) results in considerable errors at short times. Consequently, the amplitudes α_i and time constants τ_i were determined by inverse analysis, using the mean square distance over the dimensionless interval $[0, 1.2]$. Figure 5 depicts the quality of the best fit for a cylinder, with emphasis over short times. The most important discrepancy between the analytical solution and the reduced model always appears at extremely short times, but remains less than 3% in relative error. Using two exponentials reduces this error slightly in amplitude, but significantly in time interval. Tables 1 and 2 present the full set of parameters together with the residual errors, for the three geometries when using one or two exponential functions, respectively.

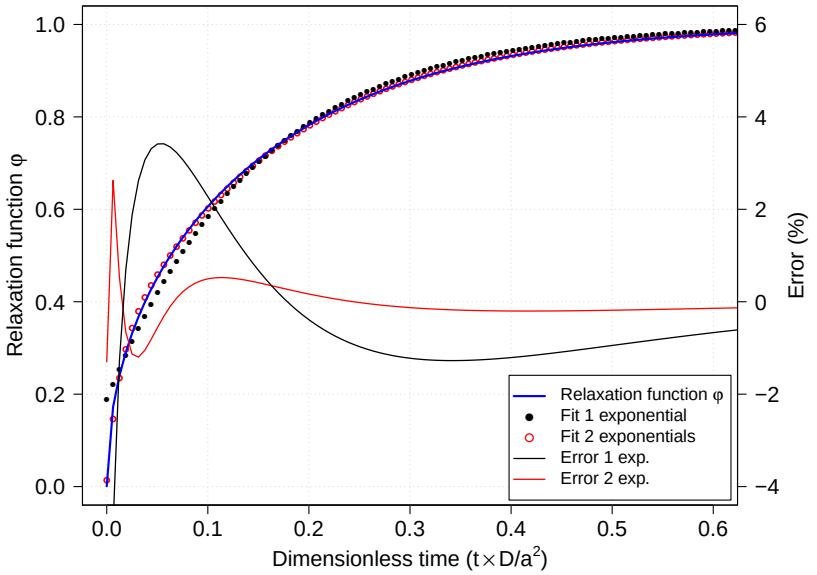

Figure 5: Approaching the relaxation function φ obtained for cylindrical inclusions by one or two exponential functions. For the reference solution to be accurate even at short times, 500 terms were considered in equation (27).

Table 2: Parameter values to approach diffusion in a simple-shape inclusion with two exponential functions (the identification was performed over the dimensionless time interval $[0, 1.2]$ and with 500 terms of the analytical solutions).

Parameters	**Plate**	**Cylinder**	**Sphere**
α_1	0.82014	0.72546	0.66819
$\tau_1/(a^2/D)$	0.40146	0.16732	0.09541
α_2	0.16064	0.26074	0.32459
$\tau_2/(a^2/D)$	0.02218	0.01208	0.00784
Norm of residues	14.10^{-4}	19.10^{-4}	15.10^{-4}

4. Accounting for memory effects in the coupled formulation

To derive the coupled set of macroscopic equations with memory effects, we begin with the conservation law for moisture. To account for the memory effect, X should be used for mass balance while X_{eq}, the variable tied to water activity a_w, should be used as the driving force. For simplicity, equation (9) is written in a compact manner herein, where q_m represents the total convective flux of moisture, and j_m is the total diffusive flux of moisture. Both terms should be evaluated using X_{eq} instead of X to obtain the local value of P_v through the water activity a_w or, for example, to compute the capillary pressure or the gradient of bound water:

$$\rho_0 \frac{\partial X}{\partial t} + \nabla \cdot (\boldsymbol{q}_m(X_{eq})) = \nabla \cdot (\boldsymbol{j}_m(X_{eq})) \tag{30}$$

Combining equations (22) and (30) allows for a mass balance equation involving only X_{eq} to be obtained:

$$\rho_0 \frac{\partial}{\partial t} \left(\int_0^t \varphi(t-\tau) \frac{\partial X_{eq}(\boldsymbol{x},\tau)}{\partial \tau} d\tau \right) + \nabla \cdot (\boldsymbol{q}_m(X_{eq})) = \nabla \cdot (\boldsymbol{j}_m(X_{eq})) \tag{31}$$

Integration by parts allows for a classical formulation with memory effects to be obtained [41, 40]:

$$\rho_0 \frac{\partial}{\partial t} \left(a X_{eq}(\boldsymbol{x},t) + \int_0^t k(t-\tau) X_{eq}(\boldsymbol{x},\tau) d\tau \right) + \nabla \cdot (\boldsymbol{q}_m(X_{eq})) = \nabla \cdot (\boldsymbol{j}_m(X_{eq})) \tag{32}$$

where

$$a = \varphi(0) \quad and \quad k = \frac{\partial \varphi}{\partial t}$$

a represents the instantaneous response of the solid moisture content when X_{eq} varies. It represents the part of the sorption behavior considered as highly rapid regarding the process time, or the moisture part stored in the gaseous phase in the case of dual-scale effects. Function k is a kernel function that tends towards 0 at $t \to \infty$ and represents the fading memory. It can be singular at $t = 0$, but must be sufficiently regular to exhibit a smooth behavior in the convolution product [35]. Obviously, the fading memory vanishes when function φ is the casual function. In this case, the convolution product disappears.

However, it is noteworthy that Equation (32) is not easy to handle for a multidimensional computational solution of coupled heat and mass transfer. The numerical implementation is much easier when the function φ can be developed as a series of decreasing exponential functions. Such a series allows for the convolution product to be transformed into internal variables, whose evolutions obey simple ODEs.

$$\varphi(t) = 1 - \sum_{i=1}^{N} \alpha_i \, exp\left(-\frac{t}{\tau_i}\right) \tag{33}$$

This expression is the sum of an instantaneous relaxation with proportion $\varphi(0) = 1 - \sum \alpha_i$ of the full change in equilibrium moisture content and a series of progressive relaxations of magnitude α_i, with relaxation time τ_i. In this case, equation (22) simplifies to

$$X(t) = X_{eq}(t) - \sum_i \left(\int_{\tau=0}^{t} \alpha_i \, exp\left(-\frac{t-\tau}{\tau_i} \right) dX_{eq} \right) = X_{eq}(t) - \sum_i \phi_i(t) \tag{34}$$

Now, we need to derive an equation that can update each internal variable $\phi_i(t)$, as defined in equation (34). Hence, we express the variation in ϕ_i between times t and $t+dt$ as follows:

$$\phi_i(\boldsymbol{x}, t+dt) = exp\left(\frac{-dt}{\tau_i} \right) \phi_i(\boldsymbol{x}, t) + \alpha_i \, dX_{eq}(\boldsymbol{x}) \tag{35}$$

The increment in equilibrium moisture content involved in this equation is the change in equilibrium due to the change in water activity between t and $t+dt$: $dX_{eq}(\boldsymbol{x}) = X_{eq}(a_w(\boldsymbol{x}, t+dt)) - X_{eq}(a_w(\boldsymbol{x}, t))$.

At each node of the computational domain, the values of the internal variables ϕ_i have to be updated using equation (35). Regardless of the reason for the memory effect, the concept of internal variable holds, provided that function φ is defined as a set of exponential functions.

In a computational code, only one variable, X or X_{eq}, should be used for the mass balance. A full formulation in X, more relevant for a mass balance equation, is possible provided a relation between dX and dX_{eq} can be derived. Such a relation can be obtained by combining equations (34) and (35):

$$dX_{eq}(1 - \sum_i \alpha_i) = dX + \sum_i \phi_i(t) \left(exp\left(-\frac{dt}{\tau_i} \right) - 1 \right) \tag{36}$$

This equation allows for the internal variables to be updated using the evolution of dX in time. However, the condition $\varphi(0) > 0$ is required for the expression (36) to be inverted, unless the averaged values over a finite time step were used. We can now propose the new set of coupled heat and mass transfer equations allowing all memory effects to be transferred at the macroscopic level:

Moisture conservation

$$\rho_0 \frac{\partial X}{\partial t} + \nabla \cdot (\rho_w \bar{\boldsymbol{v}}_w + \rho_v \bar{\boldsymbol{v}}_g) = \nabla \cdot (\rho_g \boldsymbol{f} \boldsymbol{D}_v \nabla \omega_{v,eq} + \rho_s \boldsymbol{D}_b \nabla X_{b,eq}) \tag{37}$$

Energy conservation

$$\begin{aligned} \frac{\partial}{\partial t} \left(\varepsilon_w \rho_w h_w + \varepsilon_g (\rho_v h_v + \rho_a h_a) + \overline{\rho_b h_b} + \varepsilon_s \rho_s h_s \right) \\ + \nabla \cdot (\rho_w h_w \bar{\boldsymbol{v}}_w + (\rho_w h_v + \rho_a h_a) \bar{\boldsymbol{v}}_g) \\ = \nabla \cdot (\boldsymbol{\lambda}_{eff} \nabla T + (h_v - h_a) \rho_g \boldsymbol{f} \boldsymbol{D}_v \nabla \omega_{v,eq} + h_b \boldsymbol{D}_b \nabla X_{b,eq}) \end{aligned} \tag{38}$$

Air conservation

$$\frac{\partial (\varepsilon_g \rho_a)}{\partial t} + \nabla \cdot (\rho_a \bar{\boldsymbol{v}}_g) = \nabla \cdot (\rho_g \boldsymbol{f} \boldsymbol{D}_v \nabla \omega_a) \tag{39}$$

Non local equilibrium

$$\begin{aligned} X_{eq}(\boldsymbol{x}, t) &= X(\boldsymbol{x}, t) + \sum_i \phi_i(\boldsymbol{x}, t) \\ X_{b,eq} &= min(X_{fsp}, X_{eq}) \\ \omega_{v,eq} &= \omega_v(a_w(X_{eq}, T)) \end{aligned} \tag{40}$$

Updating memory effects

$$\begin{aligned} d\phi_i &= (exp(-dt/\tau_i) - 1)\, \phi_i + \alpha_i\, dX_{eq} \\ \text{with} \quad dX_{eq} &= \frac{dX + \sum_i \phi_i(t)\, (exp\,(-dt/\tau_i) - 1)}{(1 - \sum_i \alpha_i)} \end{aligned} \tag{41}$$

This formulation represents the key theoretical outcome of the present study. It will be used and validated on several case studies in the following sections.

5. Computational simulation

5.1. Computational strategy

The macroscopic formulation requires a set of strongly coupled and non-linear equations to be solved. In the present study, simulations were computed using an in-house code, *TransPore*, written in Fortran 95. A fully coupled strategy, with block matrices, was implemented using a Newton–Raphson (NR) scheme with a variable time step. Temperature T, moisture content X and air density $\overline{\rho}_a^g$ are selected as primary variables. The Jacobian matrix was evaluated by numerical derivation. One dimensional (1-D) to three-dimensional versions of *TransPore* are available. Further details might be found in [31]. The 1-D version allows for the entire simulation to be computed in less than one second on a classic Intel-based computer (i7 at 3 GHz) for a mesh size of 50 CVs. Such a fast code allows for the use of this computational tool as a physical engine in an inverse procedure [34]. Hence, this version has been embedded in a fully graphical interface, written with the graphical library *Winteracter*. This application can be used either for simulation or for an identification to fit experimental data or simulation data such as a reference dual-scale modeling.

The task of solving the dual-scale formulation is more complicated for several reasons:

- A dual-scale approach requires the fields of all micro-models (one per mesh position of the macroscopic domain) to be updated along the macroscopic time,
- The two-way coupling between scales (evolution of boundary conditions imposed to the micro-models and source/sink terms transferred at the macroscopic level) add strong coupling and non-linearities in comparison to the macroscopic model,
- The low moisture inertia of the macroscopic phase results in an extremely stiff coupling between scales.

The first tests using an explicit coupling between the two scales confirmed the challenge. Even by artificially increasing the moisture inertia of the macroscopic phase, a full simulation required one to three days of CPU time on a classic Intel-based computer (i7 at 3 GHz), depending on the configuration. Hence, a completely new code was re-engineered (*TransPore*[2]). The master code solved the macroscopic solution. For the macroscopic version, a fully coupled NR strategy was used to handle the non-linearities. Coupling between scales is implemented in this strategy. At each macroscopic time step, the variation in the microscopic fields of all micro-models are computed along the macroscopic time step for the actual macroscopic variable values, but also by shifting each macroscopic variable. The fluxes supplied to the macro-model are averaged over the macroscopic time step. This allows for the Jacobian matrix to fully include the dual-scale coupling. With three variables, this implies that 4N calls to the micro-model are required for each non-linear iteration of the NR procedure.

The macroscopic time-step evolves along the simulation depending on the global convergence condition, whereas each micro-model continuously adapts its microscopic time-step to advance by one macroscopic time-step. Owing to this full coupling strategy, the CPU time was reduced to a few minutes (between 3 and 10 minutes depending on the configuration) for 25 CVs at the macroscopic, and 21 CVs for each micro-model. This is 500 times faster than an explicit coupling between scales.

5.2. Model parameters

All tests proposed herein are sorption tests with the LDF. As the material remains in the hygroscopic domain, all parameters related to liquid water may be discarded. In addition, the medium morphology allows for us to assume that the migration of bound water is negligible at the macroscopic level. The key parameters of the model are therefore

- the sorption isotherm defined by the Hailwood–Horrobin model [16], using the adsorption envelop curve [2]: $RH/X = 2.76 + 15.84 \times RH - 15.26 \times RH^2$,
- the thermal conductivity set at $0.05 W.m^{-2}.s^{-1}$ [30],
- the dimensionless effective water vapor diffusivity $\boldsymbol{f}$ set at 0.6 [23],
- the intrinsic permeability set at $K = 6.6.10^{-11} m^2$ [1]

The medium permeability is supposed to be small enough for the air to be at rest in the macroscopic phase. Therefore, the microscopic heat and mass exchange coefficients (h_h^σ and h_m^σ) were evaluated by assuming a parabolic diffusion equation [28]. With the small size of the pore, hence the short diffusion distances, these exchange coefficients are very large and produce boundary conditions very close to Dirichlet conditions. As a consequence, the parameters summarized in tables 1 and 2 are therefore valid to account for diffusion in the new formulation.

In addition to these key parameters, the geometrical factors and bound water diffusivity are required for the dual-scale model. The fiber diameter was determined from the morphological observations of fiberboard samples with an environmental scanning electron microscope (ESEM, FEI Quanta 200). These images show that the solid phase is primarily composed of isolated fibers with a diameter in the range of 30 to 50 μm, together with a few fiber aggregations [2]. The fibers are distributed randomly in the mat preparation but, owing to the consolidation process, their orientation is preferentially parallel to the panel face. The inclusion radius was set at $20\,\mu m$.

The source terms Q are computed as the microscopic flux density q times A_σ, the surface area of ∂V_σ. In the case of the vapor source term as follows:

$$Q_v(t,x) = \frac{A_\sigma}{|V|} q_v(t,x) \quad x \in \Omega \tag{42}$$

the geometrical factor $A_\sigma / |Y|$ (m^2/m^3) involved in equation (42) is the area of the exchange surface between phases σ and γ per unit of macroscopic volume. For the cylinders (the REV depicted in figure 2), the geometrical terms can be simply deduced from the dimension and macroscopic porosity. Table 3 summarizes the parameter values used in the simulations.

5.3. Dual-scale simulations

The dual-scale model *TransPore*^{2} was used to generate reference tests that will be used to validate the new macroscopic formulation. Hence, simple sorption tests, similar to those performed in our laboratory, were simulated:

- Uniform initial moisture content = 0.07 (water mass over dry mass),
- Uniform initial temperature = 33°C,
- External dry bulb temperature = 33°C,
- External dew point temperature = 27°C.

With the sorption isotherm of the LDF, the corresponding equilibrium moisture content is slightly higher than 0.11.

Simulations were performed using a wide range of values for the bound water diffusivity D_b^σ: 1, 3, 10, 30, and 100 $\times 10^{-14}\, m^2.s^{-1}$. Referring to the representative elementary

Table 3: Values of key parameters used in the simulations

Apparent density	$\rho_0^\gamma = 160 kg.m^{-3}$
Macroscopic diffusivity	$D_{eff}^\gamma = 0.60 \times D_v$
Macroscopic conductivity	$\lambda_{eff}^\gamma = 0.05\, W.K^{-1}.m^{-1}$
Intrinsic permeability	$K^\gamma = 6.6.10^{-11}\, m^2$
Macroscopic heat transfer coefficient	$h_h^\gamma = 25\, W.K^{-1}.m^{-2}$
Macroscopic mass transfer coefficient	$h_m^\gamma = 0.025\, m.s^{-1}$
Radius of the microscopic particle	$r = 20\, \mu m$
Density of the solid phase	$\rho_0^\sigma = 1200\, kg.m^{-3}$
Macroscopic porosity	$\varepsilon_g^\gamma = 0.87$
Geometrical factor	$A_\sigma / \lvert Y \rvert = \dfrac{2(1-\phi_{mac})}{r} = 13340$

volume (VER) specified in figure 2, the simulation were performed in 1-D Cartesian coordinates at the macroscopic scale and 1-D axisymmetrical coordinates at the microscopic scale. The macroscopic mesh comprises 25 CVs, hence 25 micro-models, with each one being defined by 21 CVs.

Figure 6 presents the two-scale moisture content fields for two contrasted values of bound water diffusivity: ($1.10^{-14}m^2.s^{-1}$ and $3.10^{-13}m^2.s^{-1}$) for a 20-mm-thick slab of the LDF. The macroscopic values of moisture content are plotted on the y-axis while the colored cylinders represent the microscopic field within each micro-model. For clarity, only one micro-model out of three is represented herein. Consistently, the MC scale is the same for the y-axis and for the color legend. In the case of fast diffusion in solid inclusions ($D_b^\sigma = 3.10^{-13}m^2.s^{-1}$, Fig. 6 top), the MC field equilibrates easily within the inclusion. In this case, the fields are almost always uniform within each inclusion (uniform color) and the macroscopic profiles in the sample thickness are classic diffusion profiles. When the diffusion in the solid inclusions is significantly reduced ($D_b^\sigma = 1.10^{-14}m^2.s^{-1}$, Fig. 6 bottom), the microscopic characteristic time is of the same order of magnitude as the macroscopic one. In this case, steep MC fields are obtained inside the inclusions and the macroscopic profiles are flatter. In particular, the moisture uptake near the exchange surface is reduced significantly. A large part of water uptake is now controlled by the resistance to the microscopic diffusion.

Figure 7 depicts the evolution of three variable values (temperature, moisture content, and relative humidity) at the core of the slab (mid-thickness) for the five values of bound water diffusivity. For comparison, the results obtained with the classical macroscopic model are also plotted in these graphs. It is noteworthy that this was computed using a completely different in-house computational code (*TransPore*) with the parameter values of Table 3 and with the same initial and boundary conditions. For $D_b^\sigma = 1.10^{-12}m^2.s^{-1}$, the diffusion inside the fibers is sufficiently fast for the dual-scale model to be extremely close to the macroscopic model. In this case, the full moisture inertia of inclusions acts at a short time. As the bound water diffusivity decreases, the gap between the dual-scale model and the classical macroscopic model increases. The difference between the macroscopic model and the dual-scale model at mid-thickness can be explained by the delaying effect of fiber inertia regarding the moisture:

- The initial temperature increase owing to reduced water condensation. At long times, the curves cross each other because the delayed inertia produces a larger demand for latent heat at long times, compared to the macroscopic model,
- As the resistances to macroscopic diffusion in the gaseous phase and to bound water diffusion in the solid phase act in series, the evolution of moisture content decelerates when the bound water diffusivity decreases. This effect becomes significant for $D_b^\sigma = 1.10^{-14}m^2.s^{-1}$,
- As a consequence of moisture inertia in the solid phase, a much faster transmission of relative humidity change toward the sample core is observed. Again, this effect becomes significant for the two largest values of D_b^σ.

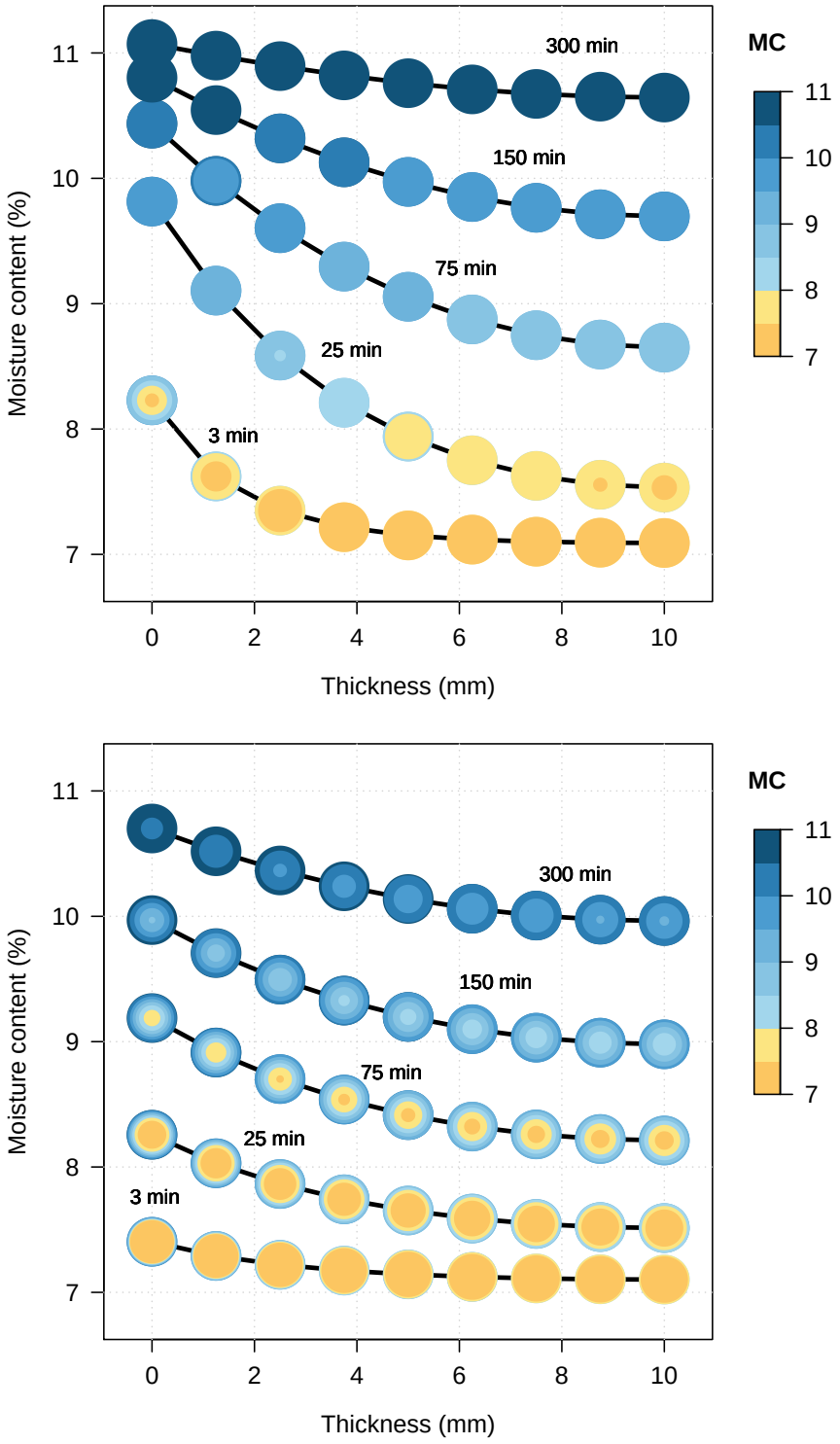

Figure 6: Dual-scale simulations for a 20-mm-thick LDF panel submitted to symmetrical boundary conditions. The effect of microscopic diffusivity on the local (fiber) and global (slab thickness) moisture content field: (top) $D_b^\sigma = 3.10^{-13} m^2.s^{-1}$ and (bottom) $D_b^\sigma = 1.10^{-14} m^2.s^{-1}$.

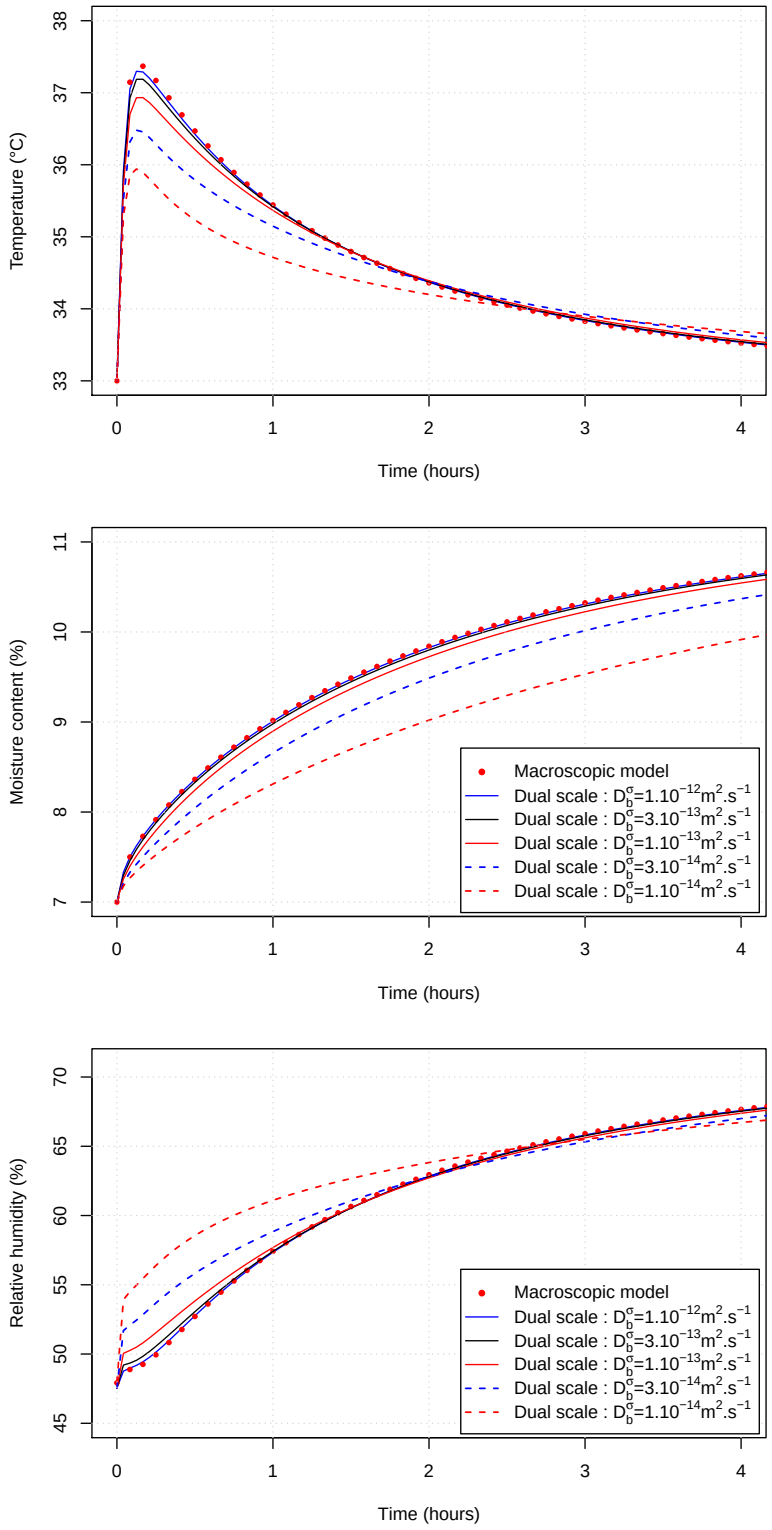

Figure 7: Dual-scale simulations for a 20-mm-thick LDF panel. Effect of microscopic diffusivity on the evolution of macroscopic variables at mid-thickness: temperature (top), moisture content (middle), and relative humidity (bottom). As expected, the dual-scale solution tends towards the classical macroscopic formulation when D_b^σ is sufficiently large.

6. Validation of the formulation with memory effects

6.1. Computational strategy

The new macroscopic formulation was implemented in the macroscopic version of the code, *TransPore*, written in Fortran 95. The same fully coupled strategy, with block matrices, together with a Newton–Raphson (NR) scheme with a variable time step is therefore adopted. To ensure a fast convergence of the non-linear and coupled set of equations, two major cautions were adopted to consider the new formulation:

- updating the memory effects (equation 28) was fully implemented in the NR procedure
- the full exponential expression of this equation, instead of a first oder approximation, was used to avoid error when the time-step is not much smaller than the smallest value of τ_i.

Thanks to this efficient computational strategy, the CPU time of the 1-D version remains similar to the classical macroscopic model. One entire simulation ranges between one and three seconds on a classic Intel-based computer (i7 at 3 GHz) for a mesh size of 50 CVs. The worse CPU time is obtained in the case of three internal variables (dual-scale effects + molecular relaxation), with a small value of τ_1 and a sum of three α_i close to the unit, which reduces dramatically the mass inertia of the medium. The new macroscopic formulation therefore represents a dramatic reduction of the CPU time, by a factor 100, compared to the full dual-scale model.

6.2. Dual-scale effects

The new formulation presented in the previous section has been validated using several case studies. We first tested the ability of the formulation to capture the dual-scale effect encountered in the case of storage inclusions placed in a conductive phase. Consistent with section 4, the diffusion into the fibers was approached by one or two exponential functions in the modified macroscopic formulation. The more severe dual-scale configuration ($D_b^\sigma = 1.10^{-14} m^2.s^{-1}$) was tested in this study. Figure 8 shows that studying diffusion using only one exponential function can capture the dual-scale effects (error less than 0.4°C for temperature , 0.05% for MC, and 2% for RH). When using two exponential functions, the prediction is quasi-perfect, except at very short times, with the error reduced to 0.1°C for temperature , 0.01% for MC, and 0.5% for RH for times greater than 10 min. These simulations confirm that the dual-scale effect can be reproduced well by the macroscopic formulation with memory effect. To obtain accuracy, we recommend the diffusion inside inclusions to be represented by two exponential functions (Table 2).

6.3. Molecular relaxation

In the macroscopic formulation, the global memory effect is treated as the sum of the contributions of each single exponential function. By incorporating molecular relaxation to the dual-scale configuration, the question arises whether two phenomena occur at different spatial scales (fiber and cell wall, as depicted in Fig. 1) can be considered as additive

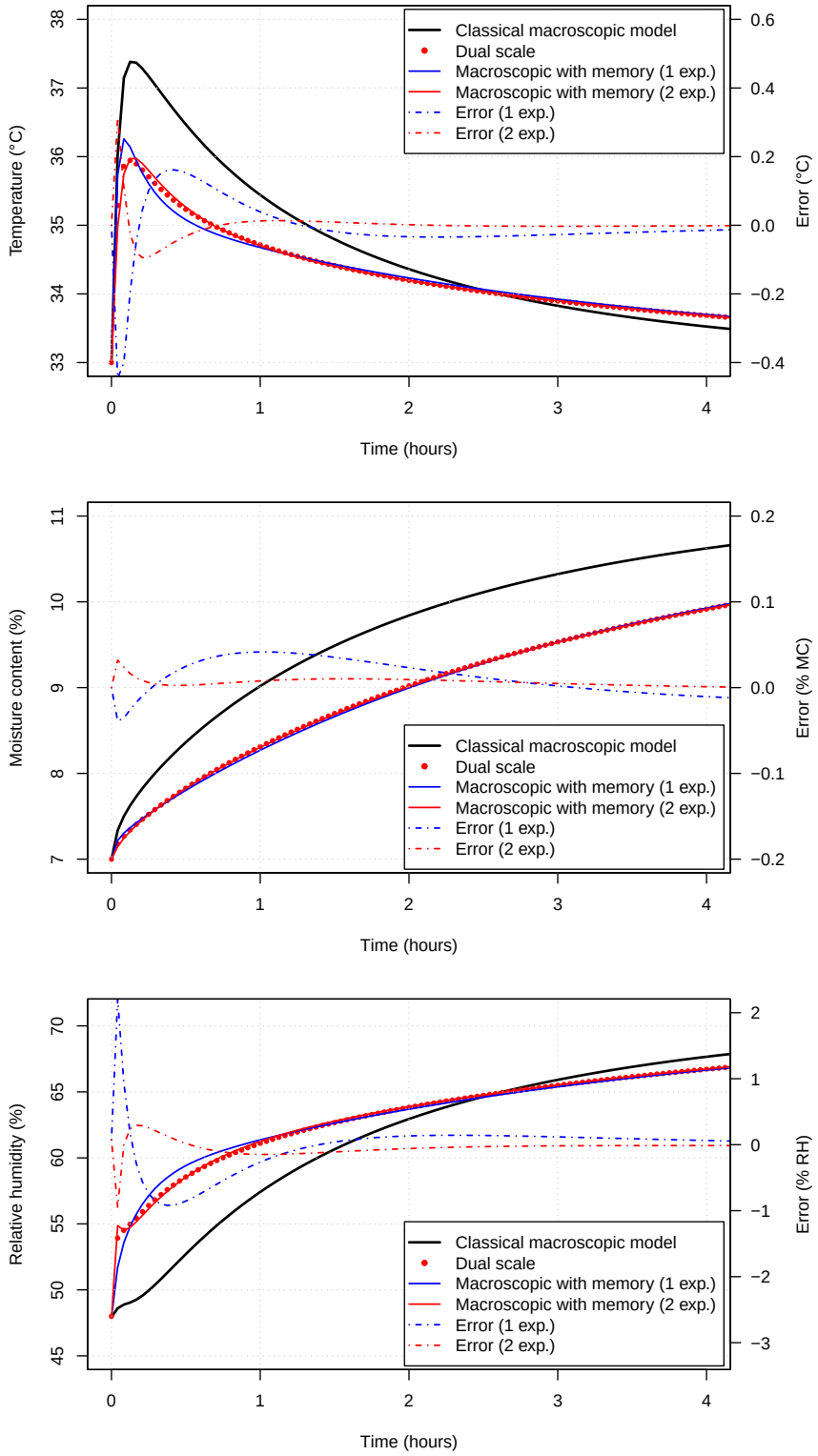

Figure 8: Ability of the novel formulation to approach the dual-scale effects using a macroscopic formulation. The worst case of figure (7), $D_b^\sigma = 1.10^{-14} m^2.s^{-1}$, was selected as a case study. The kernel function was defined either by one or two exponential functions.

effects. To address this question, the dual-scale model is mandatory. Therefore, we generated two reference solutions using *TransPore*[2]. The parameter values were chosen to obtain two contrasted values of characteristic times for fiber diffusion and molecular relaxation (Table 4).

Table 4: Parameter values selected to test the additivity of dual-scale effect and molecular relaxation.

Parameter	Case study 1	Case study 2
Non-Fickian part α	0.25	0.25
Characteristic time τ	$10^5 s$	$10^4 s$
Bound water diffusivity D_b^σ	$1.10^{-13} m^2.s^{-1}$	$1.10^{-14} m^2.s^{-1}$

In the dual-scale model, each phenomenon can be formulated at the appropriate spatial level: fiber diffusion becomes non-uniform fields inside each inclusion, whereas molecular relaxation is considered at each point inside the inclusion of each micro-model. Hence, the local time constant for molecular relaxation depends on both the position in the slab thickness and the position inside the corresponding inclusion.

To simulate the sum of two effects in the modified macroscopic formulation, the proportion of each exponential function must be changed accordingly. Because the contribution of all effects is additive, the factors set for diffusion should be corrected by the proportion of molecular relaxation. Using two exponentials for diffusion, the full expression reads

$$\varphi(t) = 1 - (1 - \alpha_{relax}) \left(\sum_{i=1}^{2} \alpha_i \, exp\left(-\frac{t}{\tau_i} \right) \right) - \alpha_{relax} exp\left(-\frac{t}{\tau_{relax}} \right) \tag{43}$$

In equation (43), α_{relax} and τ_{relax} are the parameters of function φ for molecular relaxation, while α_i and τ_i, for $i = 1, 2$, are the parameter values for diffusion, as defined in Table 2.

The corresponding simulations obtained with the full dual-scale model with molecular relaxation and with the macroscopic model with memory effects are depicted in figure 9. Case study 1 uses parameter values typical of those measured on the LDF. In this case, the time constant of molecular relaxation is much larger than the time constant of bound water diffusion. Hence, within each micro-model, the history for molecular relaxation is quasi-uniform inside the inclusion. The two mechanisms occur subsequently and are therefore perfectly additive. Consequently, it is not surprising to observe a perfect agreement between the reference test (dual-scale model) and the macroscopic model with memory effects (Fig. 9, blue curves). For case study 2, the model parameters were chosen specifically to obtain similar time constants for both phenomena (time constant of molecular relaxation divided by 10, and time constant of bound water diffusion multiplied by

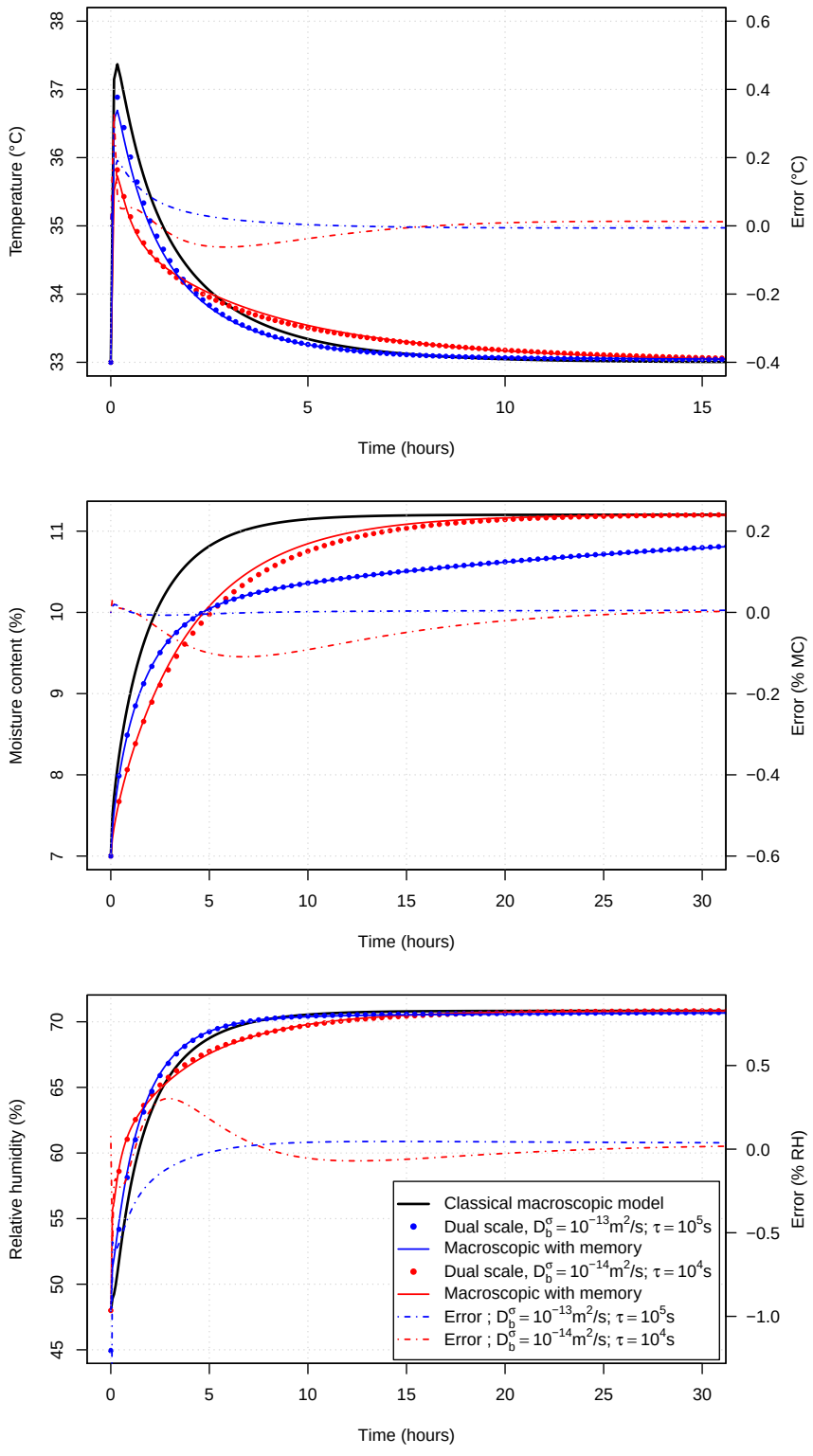

Figure 9: Ability of the novel formulation to account for memory effects arising at different spatial scales simultaneously. Two contrasted parameter sets were chosen for the time characteristics of molecular relaxation much longer than or similar to the time characteristics of microscopic diffusion.

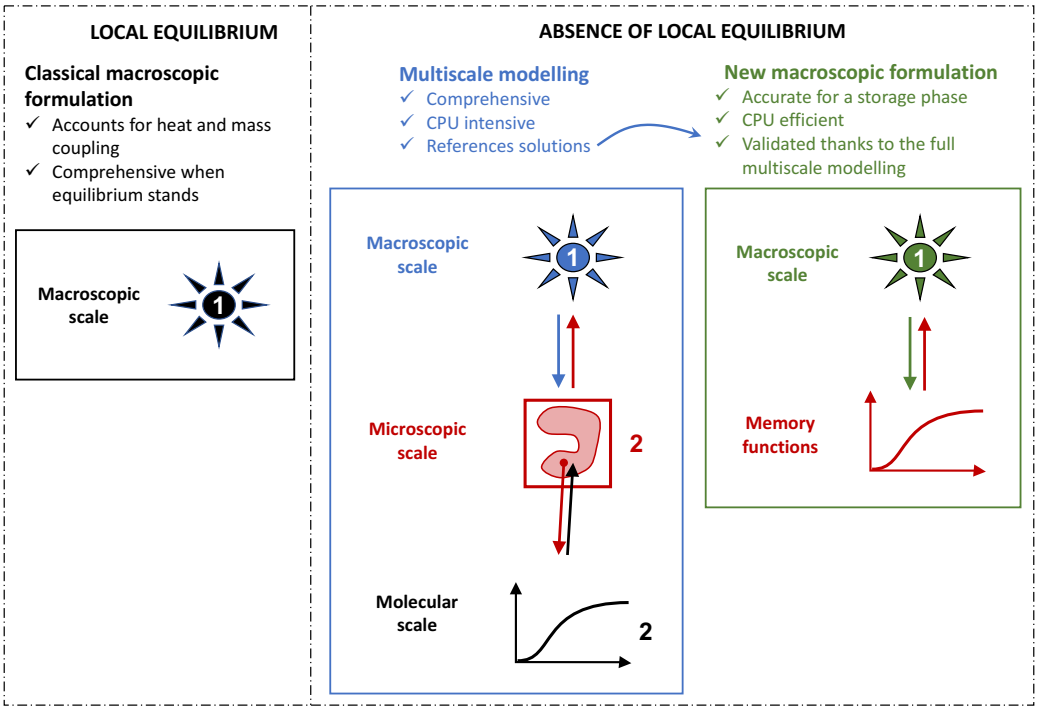

Figure 10: Summary of the present work. When the local equilibrium is not guarantee, the classical formulation of coupled heat and mass transfer fails. A full multi-scale approach is needed to account for non-local equilibrium and molecular relaxation. The new macroscopic formulation proposed in the present work allows these phenomena to be transferred at the macroscopic scale at a much reduced computational cost.

10). In this case, the macroscopic model no longer fits the dual-scale model ideally (figure 9, red curves). A small discrepancy is observed, namely for a MC between 5 and 15 h. This proves the loss of full additivity for the two phenomena arising at different spatial scales. However, the error remains extremely small: less than 0.2°C, less than 0.1% MC, and less than 0.3% RH. In conclusion, even for the extreme parameters' values, assuming both phenomena to be additive is still possible.

7. Summary

This paper presents a general and rigorous framework able to include non-local equilibrium effects in the macroscopic formulation of coupled heat and mass transfer in porous media. Its content is summarised in Figure 10. In this figure, any classical balance equation (temporal variation resulting from the divergence of fluxes) at the macroscopic level is schematised by arrows around a circle.

In the case of non-local equilibrium, several spatial scales must be considered simultaneously. A comprehensive way to do this is to use a dual scale formulation, based on the concept of distributed micro-models. Its formulation and computational strategy, needed to deal with the coupling between scales, are presented in detail. Then, the dual-scale computational model *TransPore*^{2} is used to compute reference solutions : configuration without local equilibrium, but also multi-scale modelling, where molecular relaxation is added to the dual-scale modelling at the right place (each location of the microscopic field). The coupling between the scales is always two-way, as noticed by the double arrows

in figure 10. The boundary conditions applied at a given scale comes from the variable fields of the upper scale. This allows the resulting evolution of that scale to be computed and then transferred at the upper scale as source/sink terms.

The new framework was then rigorously developed. The related computational strategy, which embeds the local history in a memory function (figure 10), was also detailed to allow the reader to include this new formulation in existing macroscopic codes. This strategy includes the development of the memory functions as a sum of exponential functions and ODEs associated to the time-evolution of the internal variables tied to these exponential functions. A series of reference solutions, computed with the comprehensive multi-scale model, allowed us to demonstrate the ability of the new formulation to accurately report diffusion inside microscopic inclusions with only two internal variables. Finally, the last section proved that two microscopic effects arising at different spatial scales (dual-scale fields and molecular relaxation) can be transferred successfully and simultaneously at the macroscopic level.

As final output of this paper, a decision tree was derived to help the reader choose the right model in the sense of the right balance between complexity and precision (Fig. 11).

The classical, yet comprehensive, formulation of coupled heat and mass transfer in porous media should be considered first. In this model, all balance equations arise at the same spatial scale. Indeed, one must have this framework in mind as background of the most sophisticated approaches. When the assumption of local equilibrium applies, the 3-variable model is comprehensive and allows a large range of configurations to be simulated, namely any "high temperature" configuration which gives rise to a gradient of the total pressure inside the medium. In some cases, this model can be simplified to the 2-variable model which still accounts for the heat and mass coupling [29].

The failure of local equilibrium is not so obvious to evidence [45]. A simple rule consists in comparing the characteristic time constants involved in the problem: time constants of macroscopic phenomena (thermal conduction, mass diffusion, bulk flow related to Darcy's law...), similar phenomena involved at the microscopic scale (transfer in fractured rocks, bound water diffusion in fibres, thermal diffusion in inclusions...) and specific phenomena such as molecular relaxation in polymers. The macroscopic phenomena depends on the product size (typically as the squared size for diffusive phenomena) while the others depend solely on the porous medium morphology and its composition. The assumption of local equilibrium requires that all macroscopic time constants be much larger than all other time constants.

If local equilibrium does not hold, a multi-scale approach is mandatory. In this case, the first question is wether the local phase might be out of equilibrium AND participate to the macroscopic fluxes. When such a situation arises, the multi-scale model should be even more complex than the concept of distributed micro-models used in this work [5]. However, most non-local equilibrium configurations are explained by a slow phase (a storage phase) generating source/sink terms. In order to apply the new framework proposed in this work, the behavior of the storage phase must be represented by a constant memory function. Indeed, if the memory function changes over time, it is no longer possible to account for the local history via a convolution product. This is the case when the porous morphology changes over time or when the microscopic boundary conditions affect the memory functions and change over time (variable fluid velocity for example).

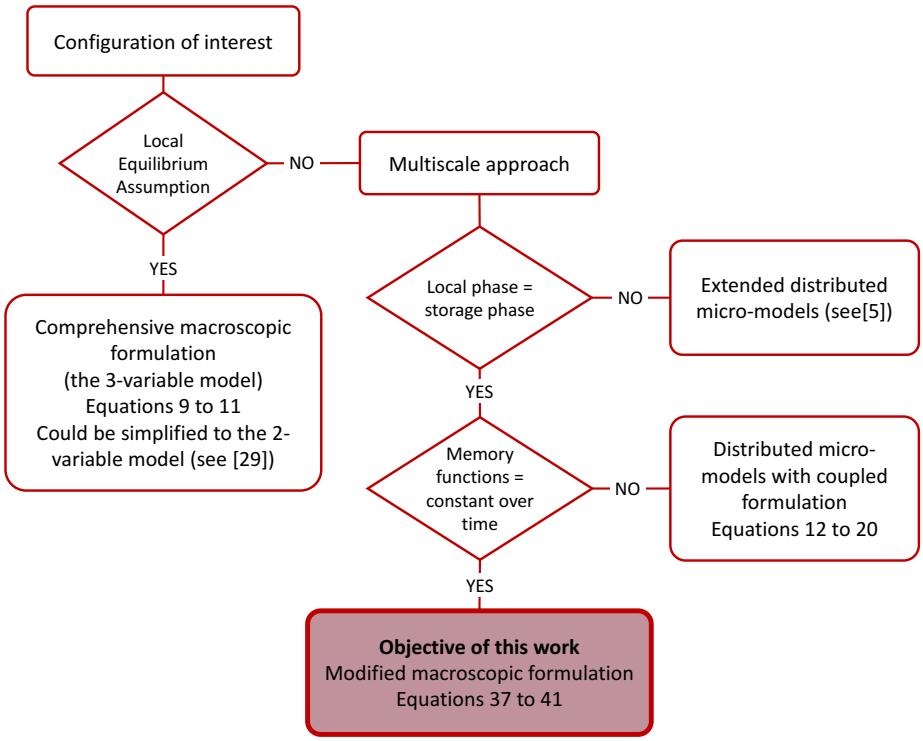

Figure 11: Identification key to choose the most appropriate coupled heat and mass transfer model (level of complexity adapted to the configuration).

The new formulation applies in the case of constant memory functions. It allows the coupling between scales to be considered with accuracy at a much lower CPU cost, with a typical gain of two orders of magnitude. However, once the decision tree goes up to the new formulation, the relevant memory functions are still to be determined. This can be done experimentally by performing experiments on very small samples. In fact, reducing the sample size allows the macroscopic time constants to become smaller than the microscopic ones and therefore to focus the sample answer on microscopic effects. In addition, small samples impose almost the same conditions at any point, which allows the memory functions to be obtained without deconvolution by applying a step function. The memory function could also be determined theoretically, either by analytical solutions in simple cases (simple geometry, linear phenomenon, simple boundary conditions) or by computational simulation. In this sense, the increasing performances of 3-D imaging and High Performance Computation make it possible to perform simulation on actual pore morphologies [23]. In the case of packed beds, the exchange between the liquid and solid phase contributes to the global resistance to transfer [44] : the boundary conditions should then be considered properly, which remains an open question. Solutions computed with classical CFD tools on real or virtual bed morphologies [39, 36] are very promising.

8. Conclusion

The primary contribution of this study was a macroscopic formulation of coupled heat and mass transfer that considered memory effects observed in lignocellulosic products. Transferring at the macroscopic level dual-scale phenomena and molecular relaxation involved a memory function that appeared as a convolution product. This new formulation

is mid-way between the classical macroscopic set of coupled transfer equations and the comprehensive, coupled, dual-scale formulation using the concept of distributed micro-models. To ease the computational solution of the set of equations, the memory function was decomposed as a series of exponential functions. Each one yielded an internal variable that obeyed a simple ODE. The incremental procedure was described clearly for an easy implementation by the reader. The three major results of the present study, validated using a full dual-scale model, are as follows:

- The dual-scale effects can be approached accurately by two exponential functions,
- Even though dual-scale mechanisms and molecular relaxation do not occur on the same scale, both can be considered at the macroscopic scale as the sum of the respective memory functions.
- The new macroscopic formulation allows relevant results to be obtained with a dramatic reduction of the CPU time (a factor 100) compared to the full dual-scale model.

The new macroscopic formulation together with the computational procedure proposed in this study may be applied to various configurations involving coupled transfers between two spatial scales. In particular, it could be applied to processes involving coupled heat and mass transfer in packed beds.

Acknowledgements

The author is grateful for the financial support of the Conseil Général de la Marne, Grand Reims and the Région Grand Est.

9. Notations

The notations are summarized in tables (5 to 7)

References

[1] W. Ai, H. Duval, F. Pierre, and P. Perre. A novel device to measure gaseous permeability over a wide range of pressures: characterisation of slip flow for Norway spruce, European beech, and wood-based materials. *Holzforschung*, 71(2):147–162, 2017. doi: 10.1515/hf-2015-0264.

[2] G. Almeida, R. Rémond, and P. Perré. Hygroscopic behaviour of lignocellulosic materials: Dataset at oscillating relative humidity variations. *Journal of Building Engineering*, 170:716–724, 2018.

[3] T. Arbogast, Jr. J. Douglas, and U. Hornung. Derivation of the double porosity model of single phase flow via homogenization theory. *SIAM Journal on Mathematical Analysis*, 21(4):823–836, 1990.

[4] T. Busser, J. Berger, A. Piot, P. Pailha, and M. Woloszyn. Dynamic experimental method for identification of hygric parameters of a hygroscopic material. *Building and Environment*, 131: 197—209, 2018.

[5] E. J. Carr, P. Perré, and I. W. Turner. The extended distributed microstructure model for gradient-driven transport: A two-scale model for bypassing effective parameters. *Journal of Computational Physics*, 327:810–829, 2016.

Table 5: List symbols (Latin letters)

Symbol	Name	Unit
a_w	sorption isotherm (water activity)	-
c	specific heat capacity	$J.kg^{-1}.K^{-1}$
D	diffusion coefficient	$m^2.s^{-1}$
f	dimensionless diffusion factor	-
h	specific enthalpy	$J.kg^{-1}$
h_h	heat transfer coefficient	$W.m^{-2}.K^{-1}$
h_m	mass transfer coefficient	$m.s^{-1}$
Δh_v	specific enthalpy of evaporation	$J.kg^{-1}$
$\boldsymbol{j}_k$	diffusive flux of component k	$kg.m^{-2}; s^{-1}$
$\boldsymbol{J}_q$	heat flux	$W.m^{-2}$
K	intrinsic permeability	m^2
$\boldsymbol{K}$	intrinsic permeability tensor	m^2
k	relative permeability	-
$\boldsymbol{k}$	relative permeability tensor	-
M	molar mass	$kg.mole^{-1}$
$\boldsymbol{n}$	normal unit vector	-
P	pressure	Pa
r	radius	m
R	gas constant	$J.kg^{-1}.K^{-1}$
R	inclusion radius	m
T	temperature	K or $°C$
V	averaging volume	m^3
$\boldsymbol{v}$	general velocity vector	$m.s^{-1}$
X	solid moisture content (dry basis)	-
bold font	vector or tensor	

Table 6: List of symbols (Greek letters)

Symbol	Name	Unit
α	pre-exponential factor	-
ε	volume fraction	-
λ	thermal conductivity	$W.m^{-1}.K^{-1}$
φ	memory function	-
ϕ	internal variable	-
μ	dynamic viscosity	$kg.m^{-1}.s^{-1}$
μ	vapour resistance ratio	-
ρ	density	$kg.m^{-3}$
τ	time constant	s
∂	partial derivative	-
∇	gradient	-
$\nabla\cdot$	divergence	-

Table 7: Subscripts and superscripts

Subscripts	Meaning
a	air
b	bound water
c	capillary
eff	effective property
eq	equilibrium
fsp	fiber saturation point
g	relative to the gaseous phase
$relax$	molecular relaxtion
v	water vapour
vs	saturated water vapour
w	liquid water
γ	macroscopic scale
σ	microscopic scale
∞	at large distance from interface

Superscript	Meaning
$\overline{\psi}$	averaged of variable ψ over the REV
$\overline{\psi}^{\ell}$	intrinsic average of ψ over phase ℓ

[6] A. Challansonnex, J. Casalinho, and P. Perré. Non-Fickian diffusion in biosourced materials: prediction of the delay between relative humidity and moisture content. *Energy and Buildings*, in press, 2019.
[7] G.N. Christensen. Sorption and Swelling within Wood Cell Walls. *Nature*, 213:782–784, 1967.
[8] J.D. Cook and R.E. Showalter. Microstructure diffusion models with secondary flux. *Journal of Mathematical Analysis and Applications*, 189:731–756, 1995.
[9] J. Crank. A theoretical investigation of the influence of molecular relaxation and internal stress on diffusion in polymers. *Journal of Polymer Science*, 11(2):151–168, 1953.
[10] J. Crank. *The mathematics of diffusion*. Oxford University Press, 1975.
[11] D. Crawley, L. Lawrie, F. Winkelmann, W. Buhl, Y. Huang, C. Pedersen, R. Strand, R. Liesen, D. Fisher, M. Witte, et al. Energyplus: creating a new-generation building energy simulation program. *Energy and buildings*, 33:319–331, 2001.
[12] J.M.P.Q. Delgado, N.M Ramos, E. Barreira, and V.P. De Freitas. A critical review of hygrothermal models used in porous building materials. *Journal of Porous Media*, 13, 2010.
[13] J.G. Downes and B.H. Mackay. Sorption kinetics of water vapor in wool fibers. *Journal of Polymer Science*, 28:45–67, 1958.
[14] L.H. Frandsen, S. Svensson, and L. Damkilde. A hysteresis model suitable for numerical simulation of moisture content in wood. *Holzforschung*, 61:175–181, 2007.
[15] W.G. Gray. A derivation of the equations for multiphase transport. *Chemival Engineering Science*, 30:229–233, 1975.
[16] A.J. Hailwood and S. Horrobin. Absorption of water by polymers: analysis in terms of a simple model. *Transactions of the Faraday Society*, 42B:84–102, 1946.
[17] U. Hornung, editor. *Homogenization and porous media*. Springer–Verlag, New York, 1997.
[18] J. Jacques, M. Labat, and M. Woloszyn. Dynamic coupling between vapour and heat transfer in wall assemblies : Analysis of measurements achieved under real climate. *Building and Environment*, 87:129–141, 2015.
[19] K. Krabbenhoft and L. Damkilde. Double porosity models for the description of water infiltration in wood. *Wood Science and Technology*, 38:641–659, 2004.
[20] H.M. Künzel, A. Holm, D. Zirkelbach, and A.N. Karagiozis. Simulation of indoor temperature and humidity conditions including hygrothermal interactions with the building envelope. *Solar Energy*, 78:554–561, 2005.
[21] J. Kwiatkowski, M. Woloszyn, and J.J. Roux. Influence of sorption isotherm hysteresis effect on indoor climate and energy demand for heating. *Applied Thermal Engineering*, 31:1050–1057, 2011.
[22] D. Lelievre, T. Colinart, and P. Glouannec. Hygrothermal behavior of bio-based building materials including hysteresis effects: Experimental and numerical analyses. *Energy and Buildings*, 84:617–627, 2014.
[23] M. Louërat, M. Ayouz, and P. Perré. Heat and moisture diffusion in spruce and wood panels computed from 3-D morphologies using the Lattice Boltzmann method. *International Journal of Thermal Sciences*, 130:471–483, 2018.
[24] U. Nyman, P.J. Gustafsson, B. Johannesson, and R. Hägglund. A numerical method for the evaluation of non-linear transient moisture flow in cellulosic materials. *International Journal for Numerical Methods in Engineering*, 66:1859–1883, 2006.
[25] W. Olek, P. Perré, and J. Weres. Implementation of a relaxation equilibrium term in the convective boundary condition for a better representation of the transient bound water diffusion in wood. *Wood science and technology*, 45:677–691, 2011.
[26] W. Olek, R. Romain, J. Weres, and P. Perré. Non-fickian moisture diffusion in thermally modified beech wood analyzed by the inverse method. *International Journal of Thermal Sciences*, 109:291–298, 2016.
[27] P. Perré. Multiscale aspects of heat and mass transfer during drying. *Transport in Porous Media*, 33:2463–2478, 2007.
[28] P. Perré. Multiscale modelling of drying as a powerful extension of the macroscopic approach: application to soid wood and biomass processing. *Dryng Technology*, 28:944–959, 2010.
[29] P. Perré. The proper use of mass diffusion equations in drying modeling: Introducing the drying intensity number. *Drying Technology*, 33:1949–1962, 2015.
[30] P. Perré and A. Challansonnex. On the importance of heat and mass transfer coupling for the

characterization of hygroscopic insulation materials. *International Journal of Heat and Mass Transfer*, 133:968–975, 2019.
[31] P. Perré and I. W. Turner. A 3D version of Transpore: a comprehensive heat and mass transfer computational model for simulating the drying of porous media. *International Journal for Heat and Mass Transfer*, 42:4501–4521, 1999.
[32] P. Perré, R. Remond, and I. W. Turner. Comprehensive drying models based on volume averaging: Background, application and perspective. In E. Tsotsas and A. S. Mujumdar, editors, *Modern Drying Technology*, volume 1. Wiley-VCH, 2007.
[33] P. Perré, R Rémond, and I Turner. A comprehensive dual-scale wood torrefaction model: Application to the analysis of thermal run-away in industrial heat treatment processes. *International Journal of Heat and Mass Transfer*, 64:838–849, 2013.
[34] P. Perré, F. Pierre, J. Casalinho, and M. Ayouz. Determination of the mass diffusion coefficient based on the relative humidity measured at the back face of the sample during unsteady regimes. *Drying Technology*, 33:1068–1075, 2015.
[35] M. Peszynska. Analysis of an integro–differential equation arising from modelling of flows with fading memory through fissured media. *Journal of Partial Differential Equations*, 8:159–173, 1995.
[36] Victor Pozzobon, Julien Colin, and Patrick Perré. Hydrodynamics of a packed bed of non-spherical polydisperse particles: A fully virtual approach validated by experiments. *Chemical Engineering Journal*, 354:126–136, 2018.
[37] R. Rémond and G. Almeida. Mass diffusivity of low-density fibreboard determined under steady- and unsteady-state conditions : Evidence of dual-scale mechanisms in the diffusion. *Wood Material Science & Engineering*, 6:23–33, 2011.
[38] R. Rémond, G. Almeida, and P. Perré. The gripped-box model: A simple and robust formulation of sorption hysteresis for lignocellulosic materials. *Construction and Building Materials*, 170:716–724, 2018.
[39] K. Salem, E. Tsotsas, and D. Mewes. Tomographic measurement of breakthrough in a packed bed adsorber. *Chemical engineering science*, 60:517–522, 2005.
[40] R. E. Showalter. Distributed microstructured models of porous media. *International Series of Numerical Mathematics*, 114:155–163, 1993.
[41] R.E. Showalter. Diffusion Models with Microstructure. *Transport in Porous Media*, 6:567–580, 1991.
[42] J.C. Slattery. *Momentum, Energy and Mass Transfer in Continua*. McGraw-Hill, New York, 1972.
[43] A. Szymkiewicz and J. Lewandowska. Micromechanical approach to unsaturated water flow in structured geomaterials by two-scale computations. *Acta Geotechnica*, 3:37–47, 2008.
[44] E. Tsotsas. Low péclet number transient heat transfer in packed beds: re-evaluation of the data of donnadieu. *Chemical Engineering Science*, 48:3434–3437, 1993.
[45] Albert J Valocchi. Validity of the local equilibrium assumption for modeling sorbing solute transport through homogeneous soils. *Water Resources Research*, 21:808–820, 1985.
[46] L. Wadsö. Describing non-Fickian water-vapour sorption in wood. *Journal of Materials Science*, 29:2367–2372, 1994.
[47] S. Whitaker. Simultaneous heat, mass and momentum transfer in porous media: a theory of drying. In J. P. Hartnett and T. F. Irvine, editors, *Advances in Heat Transfer*, volume 13, pages 119–203. Elsevier, 1977.
[48] S. Whitaker. Coupled transport in multiphase systems: a theory of drying. In Y. I. Cho J. P. Hartnett, T. F. Irvine and G. A. Greene, editors, *Advances in Heat Transfer*, volume 31, pages 1–104. Elsevier, 1998.
[49] M. Woloszyn and C. Rode. Tools for performance simulation of heat, air and moisture conditions of whole buildings. In *Building Simulation*, volume 1, pages 5–24. Springer, 2008.

LOCAL EQUILIBRIUM

Classical macroscopic formulation

- ✓ Accounts for heat and mass coupling
- ✓ Comprehensive when equilibrium stands

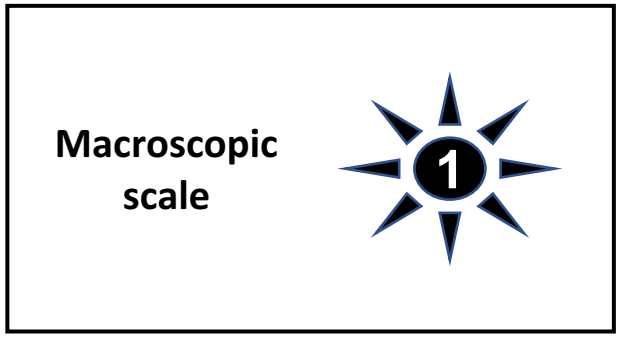

ABSENCE OF LOCAL EQUILIBRIUM

Multiscale modelling

- ✓ Comprehensive
- ✓ CPU intensive
- ✓ References solutions

New macroscopic formulation

- ✓ Accurate for a storage phase
- ✓ CPU efficient
- ✓ Validated thanks to the full multiscale modelling